Journal of Experimental Botany, Vol. 68, No. 9 pp. 2345–2360, 2017
doi:10.1093/jxb/erx085 Advance Access publication 31 March 2017
This paper is available online free of all access charges (see http://jxb.oxfordjournals.org/open_access.html for further details)

RESEARCH PAPER

Can increased leaf photosynthesis be converted into higher crop mass production? A simulation study for rice using the crop model GECROS

Xinyou Yin* and Paul C. Struik

Centre for Crop Systems Analysis, Department of Plant Sciences, Wageningen University & Research, PO Box 430, 6700 AK Wageningen, The Netherlands

* Correspondence: Xinyou.Yin@wur.nl

Received 12 June 2016; Editorial decision 27 February 2017; Accepted 27 February 2017

Editor: Greg Rebetzke, CSIRO Agriculture and Food

Abstract

Various genetic engineering routes to enhance C_3 leaf photosynthesis have been proposed to improve crop productivity. However, their potential contribution to crop productivity needs to be assessed under realistic field conditions. Using 31 year weather data, we ran the crop model GECROS for rice in tropical, subtropical, and temperate environments, to evaluate the following routes: (1) improving mesophyll conductance (g_m); (2) improving Rubisco specificity ($S_{c/o}$); (3) improving both g_m and $S_{c/o}$; (4) introducing C_4 biochemistry; (5) introducing C_4 Kranz anatomy that effectively minimizes CO_2 leakage; (6) engineering the complete C_4 mechanism; (7) engineering cyanobacterial bicarbonate transporters; (8) engineering a more elaborate cyanobacterial CO_2-concentrating mechanism (CCM) with the carboxysome in the chloroplast; and (9) a mechanism that combines the low ATP cost of the cyanobacterial CCM and the high photosynthetic capacity per unit leaf nitrogen. All routes improved crop mass production, but benefits from Routes 1, 2, and 7 were ≤10%. Benefits were higher in the presence than in the absence of drought, and under the present climate than for the climate predicted for 2050. Simulated crop mass differences resulted not only from the increased canopy photosynthesis competence but also from changes in traits such as light interception and crop senescence. The route combinations gave larger effects than the sum of the effects of the single routes, but only Route 9 could bring an advantage of ≥50% under any environmental conditions. To supercharge crop productivity, exploring a combination of routes in improving the CCM, photosynthetic capacity, and quantum efficiency is required.

Key words: Crop modelling, crop productivity, GECROS, genetic transformation, photosynthesis, radiation use efficiency, simulation, water use efficiency, yield potential.

Introduction

Yields of major crops have increased steadily during the last decades. Fischer *et al.,* (2014) claimed that, in order to ensure food and energy security for a growing and increasingly demanding population, staple crop production will need to grow by 60% from 2010 to 2050, with the greatest increases in the next 20 years. They further stressed that higher rates of increase than the current rate should be aimed for to drive faster reductions in world hunger and to guard against unanticipated negative contingencies, for example as a result of increasing frequencies of extreme weather under global climate change.

Crop yield per area of land is the production of mass per unit area multiplied by harvest index. Yield gains associated

with the first Green Revolution in cereal crops such as wheat and rice were mainly due to increased harvest index by introducing (semi-)dwarfing genes (e.g. Miflin, 2000; Sadras and Lawson, 2011). For further progress to be made, improvement in crop mass production via increasing leaf and canopy photosynthetic capacity and efficiency should be explored (Long *et al.*, 2006; Murchie *et al.*, 2009; Parry *et al.*, 2011; Ort *et al.*, 2015). Evidence suggests that genetic variation in leaf photosynthesis has not been exploited to be incorporated into crop cultivars (e.g. Driever *et al.*, 2014), except for recent releases in which yield gains were accompanied, to some extent, by traits related to increased leaf photosynthesis (Fischer *et al.*, 2014).

Arguably, exploiting natural genetic variation is still the most feasible approach to improve yield traits including photosynthesis (Flood *et al.*, 2011). For example, exploring natural variation in mesophyll conductance for CO_2 diffusion (g_m) may improve photosynthesis (Gu *et al.*, 2012; Flexas *et al.*, 2013; Chen *et al.*, 2014). However, very often there is little correlation between leaf photosynthesis and crop productivity across germplasm (Driever *et al.*, 2014; Koester *et al.*, 2016) or across individual lines of a segregating population (e.g. Gu *et al.*, 2014a, b), partly because natural variation in leaf photosynthesis and underlying traits is generally small (Driever *et al.*, 2014). To enhance crop productivity at a greater pace, genetic engineering and synthetic biology approaches to improving leaf photosynthesis should be explored (Long *et al.*, 2006, 2015; Singh *et al.*, 2014; Ort *et al.*, 2015; Kromdijk and Long 2016).

Major crops such as rice follow the pathway of C_3 photosynthesis. Compared with C_4 crops such as maize, C_3 crops have lower photosynthetic productivity primarily because ~20–35% of the carbohydrate is lost through photorespiration (Long *et al.*, 2006; Walker *et al.*, 2016), resulting from the oxygenation of ribulose-1,5-biphosphate by Rubisco, the primary enzyme for CO_2 fixation. Various genetic engineering routes to enhance C_3 leaf photosynthesis have been proposed to suppress photorespiration, thereby improving crop productivity. These include: replacing Rubisco with foreign forms with higher specificity for CO_2 relative to O_2 ($S_{c/o}$) (Whitney *et al.*, 2001; Zhu *et al.*, 2004; Parry *et al.*, 2011), designing a photorespiratory bypass (Kebeish *et al.*, 2007), and transforming the C_4 CO_2-concentrating mechanism (CCM) (e.g. von Caemmerer *et al.*, 2012) or the cyanobacterial bicarbonate-based CCM (Price *et al.*, 2011, 2013; Lin *et al.*, 2014) into main C_3 crops.

Some of the engineering approaches have already made progress and were evaluated experimentally for mass production using model plants, such as *Arabidopsis thaliana* engineered with a photorespiratory bypass (Kebeish *et al.*, 2007) and tobacco with a cyanobacterial bicarbonate transporter (Pengelly *et al.*, 2014) and with accelerated recovery from photoprotection (Kromdijk *et al.*, 2016). Any progress for major crops may not be expected in the near future, and modelling should be considered as an important tool to assess the potential of yield improvement by these photosynthesis-enhancing routes. Many researchers (e.g. Zhu *et al.*, 2004; Song *et al.*, 2013; Kromdijk and Long, 2016) have published modelling studies to assess the potential benefit of using various routes in improving photosynthesis; but most of their analyses were based on the simulation of canopy photosynthesis at a fixed leaf area index (LAI) for a given environmental condition.

During the growth cycle of annual field crops, LAI expands initially, reaches its maximum size, and then senesces, and complex interactions and feedback mechanisms can occur between photosynthesis and other physiological components (Yin and Struik, 2008). These complexities should be considered when scaling up from instantaneous leaf assimilation to daily canopy photosynthesis and to total mass production over the growing season (Boote *et al.*, 2013). To that end, Gu *et al.*, (2014*a*) ran numerical simulations using a full crop growth model, GECROS (Yin and van Laar, 2005), and examined the potential of exploiting the natural genetic variation in leaf photosynthesis within a single segregating population for contributing to crop productivity in rice (*Oryza sativa* L.) under field conditions.

Here we ran the crop model GECROS to quantify the extent to which improved leaf photosynthesis, predominantly from genetic engineering to suppress photorespiration, can result in an expected increase in crop mass production under well-watered, as well as water-limited, field conditions, using rice as an example.

Materials and methods

Model algorithms and approach in applying GECROS (v4.0) for this study are outlined below. Model parameters, if not defined in the text, are given in Table 1.

C_3 photosynthesis model

The model of Farquhar *et al.*, (1980; the FvCB model hereafter) calculates net CO_2 assimilation rate (A) as the minimum of the Rubisco-limited (A_c) and e^- transport-limited (A_j) rates. The two limiting rates can be expressed collectively as:

$$A = \frac{(C_c - \Gamma_*)x_1}{C_c + x_2} - R_d \quad (1)$$

where for A_c, $x_1 = V_{cmax}$ and $x_2 = K_{mC}(1 + O/K_{mO})$; for A_j, $x_1 = [1–f_{pseudo}/(1–f_{cyc})]J_2/4$ and $x_2 = 2O\gamma_*$, where x_1 is written according to the FvCB model extended by Yin *et al.* (2004) to be compatible with a C_4 model for which accounting for f_{cyc} is required (see later). In the model, C_c and O are the CO_2 and O_2 level, respectively, at the carboxylation sites of Rubisco, J_2 is the total PSII e^- transport rate, and Γ_*, defined as $O\gamma_*$ (where γ_* is half of the inverse of $S_{c/o}$) is the CO_2 compensation point in the absence of day respiration (R_d).

The submodel for stomatal conductance for CO_2 transfer (g_s) is:

$$g_s = g_0 + \frac{A + R_d}{C_i - C_{i*}} f_{vpd} \quad (2)$$

where g_0 is the residual value of g_s when irradiance approaches zero, C_{i*} is the intercellular CO_2 level (C_i) at which $A + R_d = 0$, and f_{vpd} is the relative effect of leaf-to-air vapour difference (VPD) on g_s (see later).

CO_2 transfer from C_a (the ambient CO_2 level) to C_c can be written as (Flexas *et al.*, 2013):

$$C_i = C_a - A\,(1/g_b + 1/g_s) \quad (3)$$

$$C_c = C_i - A/g_m \quad (4)$$

Table 1. *Input parameter values for various parts of biochemical leaf photosynthesis models*

Category	Symbol	Definition (unit)	C_3		C_4	
			Value	Reference	Value	Reference
e^- transport	Φ_{2LL}	Quantum efficiency of PSII e^- transport under limiting light (mol mol^{-1}) at T_{opt}	0.78	Yin *et al.*, (2014)	0.78	Assumed to be the same as for C_3
	$r_{2/1}$	Ratio of Φ_{2LL} to quantum efficiency of PSI e^- transport under limiting light (–)	0.85	Genty and Harbinson (1996)	0.85	Assumed to be the same as for C_3
	θ	Convexity of irradiance response of PSII e^- transport rate (–)	0.8	Yin *et al.*, (2009)	0.8	Assumed to be the same as for C_3
	f_{cyc}	Fraction of total PSI e^- flux that follows cyclic e^- transport (–)	0.05	Yin *et al.*, (2006)	0.45[a]	Yin and Struik (2012)
	f_{pseudo}	Fraction of total PSI e^- flux that follows pseudocyclic e^- transport (–)	0.10	Yin *et al.*, (2006)	0.05	Yin and Struik (2012)
	f_Q	Fraction of total plastoquinone e^- flux that follows the Q-cycle (–)	NU	NU	1	Furbank *et al.*, (1990)
	h	H^+ required per ATP production (mol mol^{-1})	NU	NU	4	Yin and Struik (2012)
	α	Fraction of O_2 evolution in bundle-sheath cells (–)	NA	NA	0.1	Standard value for C_4 species such as maize
	x	Fraction of ATP used for CCM (–)	NA	NA	0.4[a]	von Caemmerer and Furbank (1999)
	φ	Extra ATP required for the CCM per CO_2 fixed (mol mol^{-1})	NA	NA	2[a]	von Caemmerer and Furbank (1999)
	T_{opt}	Optimum temperature for Φ_{2LL} (°C)	23	Data of Yin *et al.*, (2014)	34	Data of Yin *et al.*, (2016)
	Ω	Difference between T_{opt} and the temperature at which Φ_{2LL} falls to e^{-1} of its maximum (°C)	36.8	Data of Yin *et al.*, (2014)	38.4	Data of Yin *et al.*, (2016)
Enzyme kinetics and activity	$S_{c/o25}$	Relative CO_2/O_2 specificity of Rubisco at 25 °C (mol mol^{-1})	3022	Cousins *et al.*, (2010)	2862	Cousins *et al.*, (2010)
	γ^*_{25}	Half the reciprocal of $S_{c/o25}$ (mol mol^{-1})	$0.5/S_{c/o25}$	By definition	$0.5/S_{c/o25}$	By definition
	K_{mC25}	Michaelis–Menten constant of Rubisco for CO_2 at 25 °C (µmol mol^{-1})	291	Cousins *et al.*, (2010)	485	Cousins *et al.*, (2010)
	K_{mO25}	Michaelis–Menten constant of Rubisco for O_2 at 25 °C (mmol mol^{-1})	194	Cousins *et al.*, (2010)	146	Cousins *et al.*, (2010)
	$\chi_{Vcmax25}$	Linear slope of maximum Rubisco activity at 25°C (V_{cmax25}) versus $(n–n_b)^b$ (µmol s^{-1} g^{-1})	75	Derived from data of Yin *et al.*, (2009)	93	1.24 times that for C_3 (Cousins *et al.*, 2010; Perdomo *et al.*, 2015)
	χ_{Jmax25}	Linear slope of maximum PSII e^- transport rate at 25 °C (J_{max25}) versus $(n–n_b)$ (µmol s^{-1} g^{-1})	100	Harley *et al.*, (1992); Yin *et al.*, (2009)	200	Derived from data of Yin *et al.*, (2011)
	$\chi\varepsilon_{p25}$	Linear slope of PEP carboxylation efficiency at 25 °C (ε_{p25}) versus $(n–n_b)$ (mol s^{-1} g^{-1})	NA	NA	0.791	Derived from data of Yin *et al.*, (2011)
Leaf respiration	R_{d25}	Day respiration at 25 °C (µmol m^{-2} s^{-1})	$0.01V_{cmax25}$	Common assumption	$0.01V_{cmax25}$	Assumed to be the same as for C_3
	R_m	Respiration rate occurring in mesophyll cells (µmol m^{-2} s^{-1})	NA	NA	$0.5R_d$[a]	von Caemmerer and Furbank (1999)

Table 1. *Continued*

Category	Symbol	Definition (unit)	C_3		C_4	
			Value	Reference	Value	Reference
CO_2 diffusion	g_0	Empirical residual stomatal conductance if light approaches zero (mol m^{-2} s^{-1})	0.01	Leuning (1995)	0.01	Assumed to be the same as for C_3
	a_1	Empirical constant for g_s response to VPD (–)	0.9	Derived from Morison and Gifford (1983)	0.9	Set the same as for C_3 crops[c]
	b_1	Empirical constant for g_s response to VPD (kPa^{-1})	0.15	Derived from Morison and Gifford (1983)	0.15	Set the same as for C_3 crops[c]
	χ_{gm25}	Linear slope of mesophyll conductance at 25 °C (g_{m25}) versus (n–n_b) (mol s^{-1} g^{-1})	0.125	Derived from data of Yin *et al.*, (2009); Gu *et al.*, (2012)	NU	NU
	χ_{gbs25}	Linear slope of bundle-sheath conductance at 25 °C (g_{bs25}) versus (n–n_b) (mol s^{-1} g^{-1})	NA	NA	0.007[a]	Yin *et al.*, (2011)
	u_{oc25}	Coefficient lumping diffusivities and solubilities of CO_2 and O_2 in H_2O at 25 °C	NA	NA	0.047	von Caemmerer and Furbank (1999)
Temperature response	$E\gamma_*$	Activation energy for γ_* (J mol^{-1})	24 460	Bernacchi *et al.*, (2002)	27 417	Yin *et al.*, (2016)
	E_{Vcmax}	Activation energy for V_{cmax} (J mol^{-1})	65 330	Bernacchi *et al.*, (2001)	53 400	Yin *et al.*, (2016)
	E_{KmC}	Activation energy for K_{mC} (J mol^{-1})	80 990	Bernacchi *et al.*, (2002)	35 600	Perdomo *et al.*, (2015)
	E_{KmO}	Activation energy for K_{mO} (J mol^{-1})	23 720	Bernacchi *et al.*, (2002)	15 100	Yin *et al.*, (2016)
	E_{Rd}	Activation energy for R_d (J mol^{-1})	46 390	Bernacchi *et al.*, (2001)	41 853	Yin *et al.*, (2016)
	E_{Jmax}	Activation energy for J_{max} (J mol^{-1})	88 380[d]	Yin and van Laar (2005)	116 439	Yin *et al.*, (2016)
	D_{Jmax}	Deactivation energy for J_{max} (J mol^{-1})	200 000	Harley *et al.*, (1992)	135 982	Yin *et al.*, (2016)
	S_{Jmax}	Entropy term for J_{max} (J K^{-1} mol^{-1})	650	Harley *et al.*, (1992)	458.7	Yin *et al.*, (2016)
	$E\varepsilon_p$	Activation energy for ε_p (J mol^{-1})	NA	NA	51 029	Data of Yin *et al.*, (2016)
	$D\varepsilon_p$	Deactivation energy for ε_p (J mol^{-1})	NA	NA	130 363	Data of Yin *et al.*, (2016)
	$S\varepsilon_p$	Entropy term for ε_p (J K^{-1} mol^{-1})	NA	NA	425.6	Data of Yin *et al.*, (2016)
	E_{gm}	Activation energy for g_m (J mol^{-1})	49 600	Bernacchi *et al.*, (2001)	NU	NU
	D_{gm}	Deactivation energy for g_m (J mol^{-1})	437 400	Bernacchi *et al.*, (2002)	NU	NU
	S_{gm}	Entropy term for g_m (J K^{-1} mol^{-1})	1400	Bernacchi *et al.*, (2002)	NU	NU
	E_{gbs}	Activation energy for g_{bs} (J mol^{-1})	NA	NA	116 767	Yin *et al.*, (2016)
	D_{gbs}	Deactivation energy for g_{bs} (J mol^{-1})	NA	NA	264 604	Yin *et al.*, (2016)
	S_{gbs}	Entropy term for g_{bs} (J K^{-1} mol^{-1})	NA	NA	860	Yin *et al.*, (2016)
	E_{uoc}	Activation energy for u_{oc} (J mol^{-1})	NA	NA	–1630	Yin *et al.*, (2016)
Base leaf N	n_b	Base leaf nitrogen, at and below which leaf photosynthesis is zero (g m^{-2})	0.3	Sinclair and Horie (1989)	0.3	Assumed to be the same as for C_3

NA, not applicable; NU, not used by the model presented herein.
[a] These parameter values need to be adjusted if the C_4 model is used for simulating the cyanobacterial CCM (see the text and Table 2).
[b] Where n is leaf nitrogen (g N m^{-2}); and n_b is the base leaf nitrogen, below which no leaf photosynthesis is observed.
[c] Data of Morison and Gifford (1983) showed that stomatal sensitivity to VPD could differ between C_3 and C_4; such a difference can be mimicked by our stomatal conductance model, Equation 2 for C_3 and Equation 11 for C_4 leaves, when using the same values of a_1 and b_1.
[d] Parameter set in GECROS to be dependent on crop species; the value 88 380 was set as default for rice (Yin and van Laar, 2005).

Table 2. *Nine photosynthesis-enhancing routes, the corresponding photosynthesis models, and parameter sets used for simulation in this study*

Route	Description	Model	Parameter set
1	Improved mesophyll conductance g_m	C_3	All C_3 default parameters in Table 1 but χ_{gm25} = 0.375
2	Improved Rubisco specificity $S_{c/o}$ [a]	C_3	All C_3 default parameters in Table 1 but $S_{c/o}$ = 4427
3	Improved value for both g_m and $S_{c/o}$	C_3	All C_3 default parameters in Table 1 but χ_{gm25} = 0.375 and $S_{c/o}$ = 4427
4	C_4 biochemistry introduced	C_4	All C_4 parameters (including $\chi_{Vcmax25}$ and χ_{Jmax25} [b]) in Table 1, but χ_{bs25} = 0.125
5	C_4 Kranz anatomy introduced effectively to minimize CO_2 leakage	C_4	All default C_3 enzymatic parameters plus necessary C_4 parameters to run C_4 model in Table 1, but χ_{bs25} = 0.007
6	Complete C_4 mechanism engineered	C_4	All C_4 parameters in Table 1, including low χ_{bs25} (= 0.007)
7	Only cyanobacterial bicarbonate transporters engineered	C_4	All C_3 default parameters plus necessary C_4 parameters to run C_4 model in Table 1, but χ_{gbs25} = 0.125, φ = 0.75, x = 0.2, f_{cyc} = 0.18, and $R_m = R_d$
8	More elaborate cyanobacterial CCM added	C_4	The same as Route 7, but χ_{gbs25} = 0.007
9	Complete cyanobacterial CCM engineered	C_4	The same as Route 8, but with $\chi_{Vcmax25}$ = 93 and χ_{Jmax25} = 200[c]

[a] This route assumes that crop plants are engineered to have a high $S_{c/o25}$ of the non-green alga *Griffithsia monilis* while maintaining a similar Rubisco turnover rate (Whitney *et al.*, 2001); any effect of the trade-off between Rubisco $S_{c/o}$ and carboxylase turnover rate was not quantified here, and readers are suggested to refer to Zhu *et al.*, (2014) on this effect.
[b] Based on measurements on existing maize and wheat plants, parameters $\chi_{Vcmax25}$ and χ_{Jmax25} have higher values in C_4 than in C_3 leaves (Table 1), probably reflecting the acclimation of C_4 enzymatic activities to high a CO_2 environment within the bundle-sheath compartment. While strictly speaking these higher values cannot be guaranteed for hypothetical C_4 plants of Route 4 which is not yet incorporated with the full Kranz anatomy, high values of $\chi_{Vcmax25}$ and χ_{Jmax25} for maize plants (Table 1) were used here for simulation of Route 4 in order to represent the full package of the C_4 biochemistry components.
[c] Cyanobacterial Rubisco has a higher carboxylation rate than C_3 Rubisco (Hanson *et al.*, 2016), allowing a higher investment of nitrogen in other photosynthetic protein components. However, we are not aware of the N cost for e^- transport protein components in cyanobacteria for estimating χ_{Jmax25}. For simplicity, $\chi_{Vcmax25}$ and χ_{Jmax25} for maize plants (Table 1) are used for this route, based on the expectation of engineering cyanobacterial CCM that approaches typical C_4 photosynthetic capacities (Price *et al.*, 2013).

Combining Equations 1–4 gives a standard cubic equation, as shown in Supplementary Text 1 at *JXB* online.

C_4 photosynthesis model

The C_4 model of von Caemmerer and Furbank (1999), as modified by Yin and Struik (2009, 2012), is used here. In C_4 plants, CO_2 is fixed initially in the mesophyll by phospho*enol*pyruvate (PEP) carboxylase into C_4 acids that are then decarboxylated to supply CO_2 to Rubisco, which is localized in the bundle-sheath chloroplasts. The co-ordinated functioning of the 'Kranz' anatomy and C_4 biochemistry enables an effective CCM. The extra ATP consumption for sustaining the CCM requires a higher f_{cyc} in C_4 than in C_3 photosynthesis (Yin and Struik, 2012; Nakamura *et al.*, 2013). The rate of PEP carboxylation (V_p) could be limited either by the PEP carboxylase or by the rate of e^- transport (Yin and Struik, 2009):

$$V_p = \min(\varepsilon_p C_i, x J_2 z / \varphi) \quad (5)$$

where ε_p is the initial carboxylation efficiency of the PEP carboxylase, φ is the extra ATP required for the CCM per CO_2 fixed, and z is the conversion factor of J_2 into the ATP production rate: $z = (2 + f_Q – f_{cyc})/[h(1–f_{cyc})]$ (here h is the H^+:ATP ratio; Yin *et al.*, 2004; Yin and Struik, 2012), and x represents the fraction of ATP partitioned to the reactions associated with the operation of V_p. In the standard C_4 model for malic-enzyme subtypes such as crop plants maize and sorghum, x was set to 0.4, arising from $\varphi/(3 + \varphi)$, where φ = 2, and 3 is mol ATP required for the Calvin cycle to fix 1 mol CO_2.

An effective CCM requires a small bundle-sheath conductance (g_{bs}) as g_{bs} determines the CO_2 leakage from the bundle sheath to the mesophyll (L) that affects CO_2 assimilation (von Caemmerer and Furbank, 1999):

$$L = g_{bs}(C_c - C_i) \quad (6)$$

$$A = V_p - L - R_m \quad (7)$$

Equations 5–7 can be combined to result in:

$$C_c = aC_i + (b - A - R_m)/g_{bs} \quad (8)$$

where $a = 1 + \varepsilon_p/g_{bs}$ and $b = 0$ if V_p is PEP carboxylase limited, and $a = 1$ and $b = xJ_2z/\varphi$ if V_p is e^- transport limited (Yin and Struik, 2009).

The rate of CO_2 fixation by Rubisco is modelled in the same way as for C_3 photosynthesis:

$$A = \frac{(C_c - \gamma_* O)x_1}{C_c + x_2 O + x_3} - R_d \quad (9)$$

where $x_1 = V_{cmax}$, $x_2 = K_{mC}/K_{mO}$, $x_3 = K_{mC}$ for the enzyme (Rubisco)-limited rate, and $x_1 = [1–f_{pseudo}/(1–f_{cyc})]J_2/4$, $x_2 = 2\gamma_*$, and $x_3 = 0$ for the e^- transport-limited rate. This form of the e^- transport-limited rate implies that it is the NADPH supply that causes the e^- transport limitation in C_4 photosynthesis, in comparison with the standard C_4 model in which the ATP supply was assumed to cause the e^- transport limitation (von Caemmerer and Furbank, 1999). Yin and Struik (2012) discussed the rationale that either the ATP- or the NADPH-limited form can be used for modelling C_4 photosynthesis provided that f_{cyc} and f_{pseudo} are set as appropriate. We prefer to use the NADPH-limited form here because the ATP-limited form gives $x_1 = (1–x)zJ_2/3$ (Yin *et al.*, 2011), which would predict a monotonic increase in ATP production rate, thus in an e^- transport-limited carboxylation rate, with increasing f_{cyc}. This does not agree with the more efficient CCM in terms of ATP use (e.g. cyanobacterial CCM; Price *et al.*, 2011). Using the NADPH-limited form allows a revised C_4 model to simulate photosynthesis of other CCM systems (see below) and to be consistent with the C_3 photosynthesis modelling where the NADPH-limited form is predominantly used.

A relationship for O_2 partial pressure between the intercellular air space (O_i) and the sites around Rubisco in bundle-sheath cells (O) is described as (von Caemmerer and Furbank, 1999):

$$O = \alpha A/(u_{oc} g_{bs}) + O_i \quad (10)$$

A model for g_s of C_4 leaves was formulated in a way that slightly differed from Equation 2 of the C_3 counterpart, to solve analytically for A in C_4 photosynthesis (Yin and Struik, 2009):

$$g_s = g_0 + \frac{A + R_d}{C_s - C_{s*}} f_{vpd} \quad (11)$$

where C_s is the CO_2 level at leaf surface, and C_{s*} is the C_s-based CO_2 compensation point in the absence of R_d and can be calculated as $[g_{bs}\gamma_* O_i - (1 + \gamma_*\alpha/u_{oc})R_d + R_m]/(g_{bs} + \varepsilon_p)$ (Yin and Struik, 2009). Equation 11 for C_4 and Equation 2 for C_3, although both empirical, can reproduce experimentally observed linear relationships between A and g_s across various levels of irradiance and nutrients (e.g. Wong *et al.*, 1985) (see Supplementary Fig. S1).

Equation 3 also applies to C_4 photosynthesis. Combining Equations 3 and 8–11 can yield the standard cubic equation that gives the prediction of A (Supplementary Text 1).

Algorithms common to C_3 and C_4 photosynthesis

Some common algorithms were used for C_3 and C_4 models. First, J_2 is described as a function of absorbed irradiance I_{abs} as (Yin *et al.*, 2006; Yin and Struik, 2012):

$$J_2 = \left(\alpha_{2LL} I_{abs} + J_{max} - \sqrt{(\alpha_{2LL} I_{abs} + J_{max})^2 - 4\theta J_{max}\alpha_{2LL} I_{abs}}\right)/(2\theta) \quad (12)$$

$$\text{with } \alpha_{2LL} = \Phi_{2LL}(1 - f_{cyc})/(1 - f_{cyc} + r_{2/1})$$

Equation 12 differs from the equation used in the standard FvCB model, in that f_{cyc}, Φ_{2LL}, and $r_{2/1}$ are introduced. We consider Equation 12 as a better choice as it accounts for the decrease of the overall noncyclic e^- transport efficiency (α_{2LL}) with increasing cyclic e^- transport, which runs at a higher rate in cases involving the CCM.

Secondly, in the g_s model, f_{vpd} is the function for the effect of VPD, which may be described phenomenologically as (Yin and Struik, 2009):

$$f_{vpd} = \frac{1}{\frac{1}{\max(a_1 - b_1 \cdot VPD,\ 0.01)} - 1} \quad (13)$$

where a_1 and b_1 represent the C_i:C_a ratio in water vapour-saturated air and the slope of the decrease of this ratio with increasing VPD, respectively, if g_0 in Equation 2 or 11 approaches nil.

Thirdly, a number of parameters are related to leaf temperature (T_l), and some of these can be described by the Arrhenius equation normalized with respect to 25 °C:

$$\text{Parameter} = \text{Parameter}_{25} \cdot e^{\left(\frac{1}{298} - \frac{1}{273+T_l}\right)\frac{E}{R}} \quad (14)$$

where R is the universal gas constant (8.314 J K^{-1} mol^{-1}). Equation 14 applies to R_d, γ_*, V_{cmax}, K_{mC}, K_{mO}, and u_{oc}. The temperature response of J_{max}, ε_p, g_m, and g_{bs} is described by the modified Arrhenius equation:

$$\text{Parameter} = \text{Parameter}_{25} \cdot e^{\left(\frac{1}{298} - \frac{1}{273+T_l}\right)\frac{E}{R}} \cdot \frac{1 + e^{(S-D/298)/R}}{1 + e^{[S-D/(273+T_l)]/R}} \quad (15)$$

Fourthly, the values at 25 °C of parameters V_{cmax}, J_{max}, ε_p, g_m, and g_{bs} can be further quantified as a linear function of leaf nitrogen (N) content (n) above a certain base value (n_b):

$$\text{Parameter}_{25} = \chi(n - n_b) \quad (16)$$

where χ has different values for different parameters (e.g. Harley *et al.*, 1992; Yin *et al.*, 2011). We estimated $\chi_{Vcmax25}$ for C_3 leaves from existing data and then projected to C_4 leaves (Table 1), based on the reported higher catalytic turnover rate of C_4 Rubisco than that of C_3 Rubisco (Seemann *et al.*, 1984; Sage, 2002; Cousins *et al.*, 2010; Perdomo *et al.*, 2015). There is less information about the difference in χ_{Jmax25} between C_3 and C_4 types, but our χ_{Jmax25} estimates (Table 1) are in line with Makino *et al.*, (2003), who reported a considerably higher photosynthetic N use efficiency under saturated CO_2 conditions in C_4 than in C_3 leaves.

Fifthly, experimental evidence suggests that Φ_{2LL} responds to temperature (Bernacchi *et al.*, 2003; Yin *et al.*, 2014). Due to the lack of understanding of this response, we empirically express the factor for the temperature effect, using a normal distribution alike equation (June *et al.*, 2004):

$$F_{T\Phi 2LL} = e^{-[(T_l - T_{opt})/\Omega]^2} \quad (17)$$

Finally, Equations 14, 15, and 17 require T_l, and T_l is solved from coupled modelling of leaf photosynthesis and transpiration: the algorithms in Supplementary Text 1 solve A and g_s simultaneously; the obtained g_s is used as input to the Penman–Monteith equation (Monteith, 1973; Goudriaan and van Laar, 1994) to solve leaf transpiration and T_l. This procedure involves iterations, in which T_l is initially set to be the same as the air temperature and then the solved T_l is used for re-calculating A, g_s, and leaf transpiration (Yin and van Laar, 2005).

Revising the C_4 model for simulating the cyanobacterial CCM

The single-cell C_4 photosynthesis model of von Caemmerer and Furbank (2003; see also Supplementary Text 2) can be used for simulating cyanobacterial photosynthesis (Price *et al.*, 2011). However, this model is hard to solve once it is coupled to a g_s model (Equation 2 or 11). We therefore revise the above C_4 model to simulate the cyanobacterial CCM, based on the model concept of Price *et al.* (2011). These revisions are: (i) set g_{bs} to a high value to mimic g_{ch} (conductance of the chloroplast envelope to CO_2); (ii) set V_p as if it stands for the combined rate of cyanobacterial bicarbonate transporters; (iii) set $R_m = R_d$; and (iv) re-estimate f_{cyc} and x, in view of the fact that extra ATP required for the cyanobacterial CCM also comes from the cyclic e^- pathway (Shikanai, 2007). The ATP cost of bicarbonate transport may be lower than that of the C_4 CCM (Price *et al.*, 2013; Furbank *et al.*, 2015). Two single-gene transporters (BicA and SbtA) that have been well characterized in cyanobacteria are considered here, and Price *et al.* (2011) estimated that the two transporters require 0.25 and 0.50 ATP per transport event, respectively (so, φ in Equation 5 is 0.75). We re-estimated x as 0.2 and f_{cyc} as 0.18 (Table 1), where 0.2 arises from 0.75/(3 + 0.75), and 0.18 arises from the C_4 model of Yin and Struik (2009) for the balanced NADPH:ATP ratio assuming $h = 4$. This revised C_4 model gives simulated rates of A virtually identical to the model of Price *et al.*, (2011) using the same set of parameter values (Supplementary Text 2) under normal and elevated [CO_2] conditions.

Setting scenarios of improved leaf photosynthesis for simulation

Major routes in enhancing photosynthesis will be examined, except for the photorespiratory bypass. Modelling this bypass would require more complicated algorithms and parameters (von Caemmerer, 2013), which cannot be straightforwardly implemented to simulate field environments where modelling of g_s is also needed. We examined the impact of improving g_m (Tholen *et al.*, 2012; Flexas *et al.*, 2013), improving $S_{c/o}$ (Zhu *et al.*, 2004; Parry *et al.*, 2011), introducing the C_4 mechanisms into C_3 crops (von Caemmerer *et al.*, 2012), and using cyanobacterial bicarbonate transporters and the CCM (Price *et al.*, 2011, 2013). Given that efforts to engineer these routes, especially the latter two, into new crops will most probably make progress step-wise, we propose the following nine routes (Table 2):

(1) Improving g_m, where the slope of g_{m25} versus leaf N (χ_{gm25}; see Equation 16) is set from its default value 0.125 (Table 1) to be three times higher (i.e. 0.375).

(2) Improving $S_{c/o}$, where $S_{c/o25}$ is set from its C_3 default value 3022 (Table 1) to 4427, the observed $S_{c/o25}$ for the non-green alga *Griffithsia monilis* (Whitney *et al.*, 2001).
(3) Improving g_m as well as $S_{c/o}$, where χ_{gm25} of 0.375 and $S_{c/o25}$ of 4427 are combined.
(4) Introducing C_4 biochemistry, where the C_4 photosynthesis model is used with C_4 kinetic constants (Table 1) while setting g_{bs} as high as the C_3 default g_m (i.e. setting the slope of g_{bs25} versus leaf N; χ_{gbs25}; see Equation 16) to 0.125.
(5) Making C_4 Kranz anatomy function effectively to minimize CO_2 leakage, where the low χ_{gbs25} (0.007) is combined with C_3 enzyme kinetic constants (Table 1).
(6) Engineering the complete C_4 mechanism, where C_4 kinetic constants (Table 1) combined with a low χ_{gbs25} (0.007) is used in the C_4 photosynthesis model.
(7) Engineering cyanobacterial single-subunit bicarbonate transporters (BicA and SbtA), where the above revised C_4 model is combined with the default C_3 parameters with $\chi_{gbs25} = 0.125$ and the revised values for φ, x, R_m, and f_{cyc} (Table 2).
(8) Adding a more elaborate cyanobacterial CCM, whereby the carboxysome shell proteins are expressed in chloroplasts to enrich the CO_2 level around Rubisco similar to the level in the C_4 bundle-sheath compartment. This route assumes that the chloroplastic C_3 Rubisco can be reorganized into effective carboxysome structures and other requirements for carboxysome to function are optimized (Price *et al.*, 2011). So, the same model and parameter values as for Route 7 are used, except for χ_{gbs25} which is now set to a lower value of 0.007 as for C_4 bundle-sheath conductance.
(9) A complete cyanobacterial CCM installed. The complete cyanobacterial CCM will require replacement of the C_3 Rubisco with a cyanobacterial Rubisco in order to take advantage of better kinetic properties in a high-CO_2 carboxysome (Long *et al.*, 2016). Based on the expectation of engineering the cyanobacterial CCM that approaches photosynthetic capacities typical of C_4 plants (Price *et al.*, 2013), we used $\chi_{Vcmax25}$ and χ_{Jmax25} of C_4 photosynthesis (Table 1) for this route. So, this route has the low ATP cost of the cyanobacterial CCM as well as a high enzymatic capacity per unit N to mimic the complete cyanobacterial CCM.

Simulation results of all nine routes will be compared with those of the default in which the C_3 photosynthesis model with the C_3 parameter values in Table 1 is used.

Modelling daily canopy photosynthesis and transpiration

In GECROS, instantaneous canopy photosynthesis and transpiration were calculated using the sun/shade model of de Pury and Farquhar (1997), in which the sunlit and shaded portions of the canopy each are considered as a big leaf, and the above leaf-level model is applied. Assuming an exponential profile of leaf N, total photosynthetically active N for each portion was calculated, and N-dependent photosynthetic parameters V_{cmax}, J_{max}, g_m, g_{bs}, and ε_p (see Equation 16) were then scaled up accordingly to each portion of the canopy. Instantaneous rates were scaled up to daily total, using the Gaussian integration (Goudriaan, 1986) to account for any asymmetric diurnal courses of radiation and temperature. These approaches for spatial and temporal extensions apply to the case in the absence of water limitation.

In the presence of water limitation, the available water is partitioned between sunlit and shaded leaves according to the relative share of their potential transpiration (E_p) to obtain their actual transpiration (E_a). The diurnal course of available water is assumed to follow that of radiation. Based on the Penman–Monteith equation, the actual transpiration is transformed into the actual level of stomatal resistance to water vapour ($r_{sw,a}$) (Yin and van Laar, 2005):

$$r_{sw,a} = \left(E_p - E_a\right)\left(s r_{bh} + \gamma r_{bw}\right) / \left(\gamma E_a\right) + r_{sw,p} E_p / E_a \qquad (18)$$

where $r_{sw,p}$ is the stomatal resistance to water vapour in the absence of water limitation [= $1/(1.6g_s)$, where g_s is solved from the algorithm in Supplementary Text 1]; r_{bh} and r_{bw} are the boundary-layer resistance to heat and to water vapour, respectively; γ is the psychrometric constant; and s is the slope of the saturated vapour pressure as a function of temperature (kPa °C^{-1}). The actual $r_{sw,a}$ was converted into the actual g_s, which can be used as input to the analytical quadratic model (see Supplementary Text 3) to estimate the instantaneous actual photosynthesis of the sunlit and shaded leaves. The Gaussian integration was again used to obtain the daily total of the actual photosynthesis. Equation 18 suggests that the impact of water deficit is mainly via stomatal conductance; any non-stomatal effect of water deficit is not modelled in GECROS, except when accounting for changes in T_l under drought.

Crop simulation approaches

Simulations were conducted for three sites, Los Baños (14°6'N, 121°9'E; the Philippines), Nanjing (32°56'N, 118°59'E; China), and Shizukuishi (39°41'N, 140°57'E; Japan), representing tropical, subtropical, and temperate rice-growing conditions, respectively, using 31 year (1980–2010) baseline weather data and the present atmospheric [CO_2] of 400 µmol mol^{-1}. We also ran the model under the climate scenario for 2050, at which the expected [CO_2] is ~550 µmol mol^{-1} and air temperature is 2 °C higher than the baseline (Li *et al.*, 2015). As we only examined the impact of changed leaf photosynthesis on crop productivity, we decoupled the GECROS soil module and used only the crop module for simulation to avoid any confounding effects from uncertainties in simulating soil processes. Potential production was simulated by setting the daily water supply to the crop as non-limiting. Water-limited production was simulated by setting the daily available water for evapotranspiration to no more than 50% of seasonal average daily transpiration simulated for the potential production, which was 1.97, 1.63, and 1.34 mm H_2O d^{-1} for Los Baños, Nanjing, and Shizukuishi, respectively. Daily N supply was set in such a way that the accumulated N uptake by the crop followed the sigmoid curve of Yin *et al.* (2003) and that the total uptake at maturity reached 20 g N m^{-2}, equivalent to the N uptake in high-yielding rice experiments (Setter *et al.*, 1994).

Model parameters for phenology were calibrated (Table 3) so that simulated baseline crop duration was in line with that of the standard cultivar at each site (Li *et al.*, 2015). Crop models are less accurate in predicting spikelet number and therefore harvest index than in predicting crop mass (Boote *et al.*, 2013; Li *et al.*, 2015). To minimize the impact of this uncertainty, we used the simulated total shoot mass (excluding dead leaves) at maturity as the proxy for crop productivity. Input parameters were set as the default values of GECROS for rice (Yin and van Laar, 2005) and those relevant to our study are given in Table 3. As C_4 enzyme kinetic parameters, especially their temperature responses, are less certain than the C_3 counterparts (Boyd *et al.*, 2015), additional analysis was conducted for C_4 simulation (Supplementary Text 4). Similarly, because the exact ATP cost of bicarbonate transport is uncertain (Fridlyand *et al.*, 1996; McGrath and Long, 2014), sensitivity analysis was conducted for Route 9 with regard to this cost (Supplementary Text 5). Further details about GECROS are given in Supplementary Text 6, and source codes of the full GECROS model can be obtained upon request.

Results and Discussion

Simulated leaf photosynthesis

All routes could increase A in the light-saturated region, especially Routes 6 and 9 (Fig. 1). In the light-limited region, the impact of the routes was smaller, and Routes 4, 5, and 6 in fact had a negative effect (see the inset of Fig. 1). This negative impact

Table 3. *Values of some input parameters of the GECROS crop model relevant to this study*

Parameter	Definition (unit)	Value
S_{la}	Specific leaf area constant for newly emerging leaves (m^2 g^{-1})	0.03
n_{Rmin}	Base value of root nitrogen concentration (g g^{-1})	0.005
n_{Smin}	Base value of stem nitrogen concentration (g g^{-1})	0.005
n_{RV}	Nitrogen concentration in plant reserves (g g^{-1})	0.0015
S_W	Potential weight of a single grain (g)	0.025
n_{SO}	Potential nitrogen concentration in grains (g g^{-1})	0.0145
H_{max}	Maximum final plant height (m)	1.0
TC_S	Time constant for senescence (d)	2
T_b	Base temperature for phenology (°C)	8
T_o	Optimum temperature for phenology (°C)	30
T_c	Ceiling temperature for phenology (°C)	42
m_V	Minimum number of days for pre-flowering period (thermal day[a])	70, 85, 48[b]
m_R	Minimum number of days for post-flowering period (thermal day)	28, 32, 22[b]
STTIME	Starting time of simulation, equivalent to day number (from 1 January) for seedling emergence	10, 145, 125[b]

[a] One thermal day is equivalent to one calendar day if the temperature at each moment of the day is always at the optimum.
[b] Values used for Los Baños (the Philippines), Nanjing (China), and Shizukuishi (Japan), respectively. The STTIME value for Los Baños is for the dry season there (which is the season with the high yield potential), and that for Nanjing is for single-cropping rice (that is predominant in the region, compared with the double-cropping rice where rice is planted twice per year).

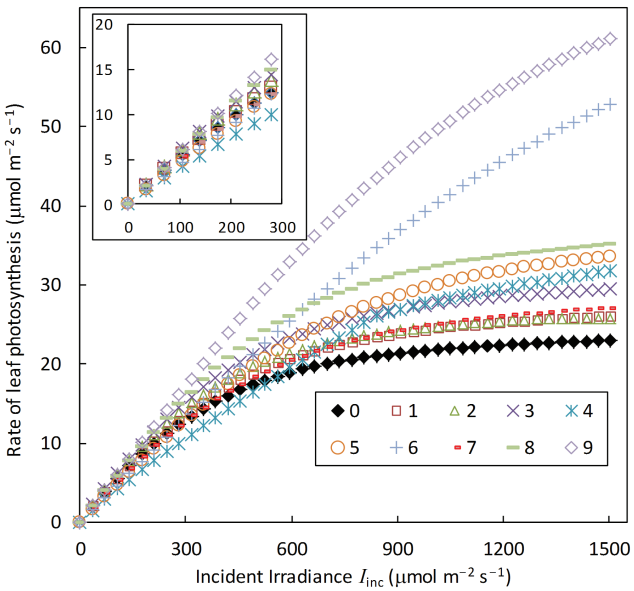

Fig. 1. Calculated leaf photosynthesis of the default C_3 (0) and nine (1–9) photosynthesis-enhancing routes in response to incident irradiance (I_{inc}). The calculation was made using the model described in the text, based on parameter values listed in Tables 1 and 2 and the following input conditions: C_a = 400 μmol mol^{-1}, T_l = 25 °C, leaf nitrogen content n = 2.3 g m^{-2}, n_b = 0.3 g m^{-2}, VPD = 2.0 kPa, and leaf photosynthetic absorptance = 0.85. The inset is for the same response curves when I_{inc} is <300 μmol m^{-2} s^{-1}.

is associated with the two extra ATPs required for PEP regeneration in the C_4 cycle (von Caemmerer and Furbank, 1999), for which a high f_{cyc} is required (Yin and Struik, 2012; Table 1). In Route 4 where this high ATP cost was not compensated by an effective CCM to suppress photorespiration, the negative effect was particularly high. Because these routes act differently for the light-saturated and limited regions, the curvature in the light response curve was diverse (Fig. 1) despite the same curvature factor θ (0.8; Table 1) used for Equation 12 describing the light response of PSII e^- transport rate for all these curves.

Simulated canopy photosynthesis

Not surprisingly, the calculated daily canopy photosynthesis ($A_{canopy,d}$) increased with increasing LAI (Fig. 2), due to a higher interception of photosynthetically active radiation (PAR) at higher LAI. Also, the light response curve of $A_{canopy,d}$ became increasingly linear with increasing LAI, because at high LAI, leaves in the canopy are predominantly light limited, and within the light-limited range leaf photosynthesis increases almost linearly with light level (Fig. 1). Because the difference in leaf photosynthesis among the routes was mainly recognized in the light-saturated region (Fig. 1), the ratio of $A_{canopy,d}$ of photosynthesis-enhancing routes to that of the default C_3 route increased with increasing radiation level, and decreased with increasing LAI (Fig. 2). $A_{canopy,d}$ of Route 4, compared with the default C_3 route, was notably lower, regardless of the radiation level, when LAI was ≥3 (Fig. 2).

Default simulation for crop durations and mass production

Using GECROS, we simulated crop duration and mass production. A 2 °C warming for 2050, relative to the present climate, was simulated to shorten crop duration by ~5, 10, and 20 d, for tropical, subtropical, and temperate environments, respectively (Table 4). This different effect across the environments is due to the fact that temperature during the growing season in the tropics is around the optimum value, at which warming is expected to have a smaller effect than at the other sites where the growing season temperature is mostly in the range where development rate increases greatly with warming.

Despite the shorter duration, simulated aboveground mass at crop maturity increased for 2050 compared with the present climate (Table 4), largely due to CO_2 elevation from 400 μmol mol^{-1} to 550 μmol mol^{-1}. This is because we implicitly

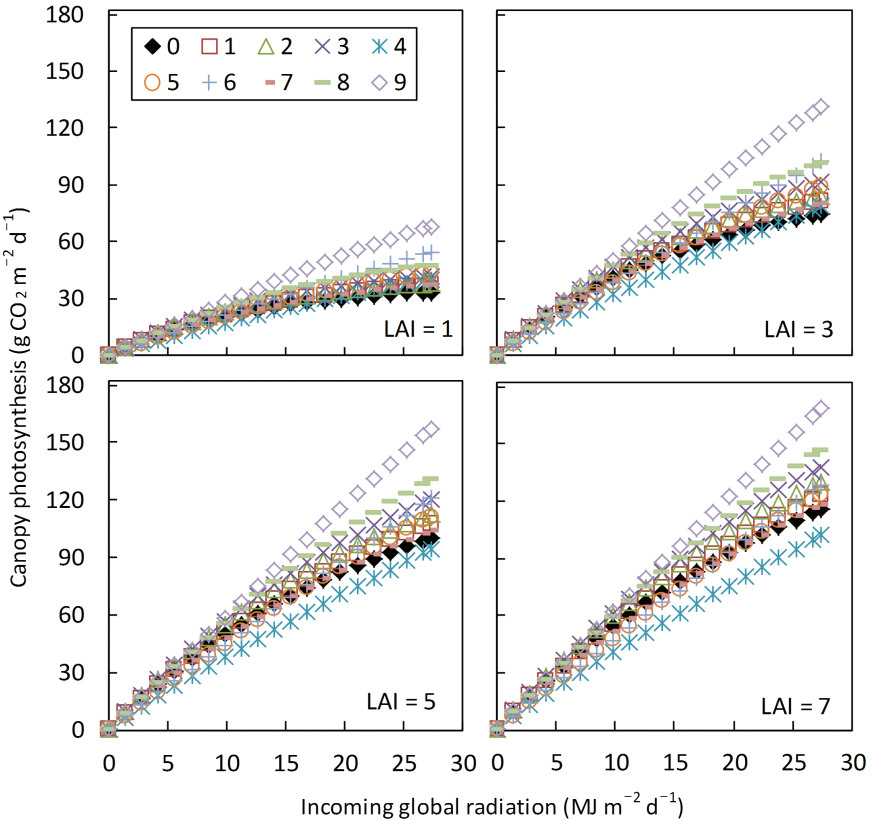

Fig. 2. Calculated daily canopy photosynthesis of the default C_3 (0) and nine (1–9) photosynthesis-enhancing routes in response to daily incoming global solar radiation, for four different sizes of canopy [leaf area index (LAI) = 1, 3, 5, and 7, respectively]. The calculation was made using the model described in the text, based on parameter values listed in Tables 1 and 2 and the following input conditions: C_a = 400 μmol mol^{-1}, T_i = 25 °C, canopy average leaf nitrogen = 2.3 g m^{-2}, n_b = 0.3 g m^{-2}, VPD = 2.0 kPa, daylength = 13 h d^{-1}, fraction of diffuse irradiance = 0.2, and canopy average leaf angle (from horizontal) = 65 °. Light extinction coefficient and nitrogen extinction coefficient required for the canopy photosynthesis model were calculated using the formulae as in GECROS with leaf scattering coefficient of 0.2 for PAR.

assumed that future breeding can develop rice cultivars capable of coping with any effect of warming on spikelet sterility, so the effect of CO_2 elevation was dominant. However, a recent FACE (free-air CO_2 enrichment) study (Cai *et al.*, 2016) using a present cultivar showed that yields of rice were decreased by 17–35% under the combination of elevated CO_2 and temperature, compared with the ambient condition, due to fewer filled grains at the elevated temperature. As expected, water limitation decreased mass production, but increased water use efficiency (WUE) (Table 4). The WUE differed little among the three sites, but was higher for 2050 than for the present climate, partly due to increased $A_{canopy,d}$ and partly due to generally decreased canopy transpiration under the 2050 climate (Table 4). The reduced canopy transpiration for the 2050 climate was largely a result of partial stomatal closure induced by higher [CO_2] (e.g. Wong *et al.*, 1985).

Impact of photosynthesis-enhancing routes on crop mass production

Compared with the default C_3 photosynthesis, all routes increased aboveground mass production, except for three cases for the potential production–2050 climate combination where the benefit from Route 5 was virtually nil or slightly negative (Table 5). In general, the benefit from Routes 1, 2, and 7 was ≤10%. All routes resulted in higher benefits in the presence of drought than in the absence of drought, and under the present climate than for 2050. This could be explained by the shape of a diminishing return for A–C_i curves, because drought and the present climate both result in a lower C_i compared with the potential production level and the 2050 climate, respectively.

Route combinations had an equal effect to, or a larger effect than, the sum of the routes acting alone. For example, the benefit from Route 3 (improving both g_m and $S_{c/o}$) was about the sum of the benefits from Route 1 (improving g_m) and Route 2 (improving $S_{c/o}$) for the potential production and was higher than the sum of the two for the water-limited condition (Table 5).

The benefit from Route 6 (the complete C_4 mechanism) was considerably higher than the sum of the benefits from Route 4 (C_4 biochemistry components) and Route 5 (Kranz anatomy components for low g_{bs}) for any condition (Table 5). This result suggests that the ongoing programme of installing C_4 photosynthesis into C_3 crops (von Caemmerer *et al.*, 2012), if successful, needs to engineer the complete C_4 mechanism. The benefit of a partial engineering is only marginal or even counter-productive under future high-CO_2 environments (see Route 5 in Table 5), because of the high ATP cost for operating the C_4 cycle. In an earlier preliminary simulation analysis

Table 4. *Days from seedling emergence to flowering and to maturity, aboveground mass at maturity, and season-long canopy photosynthesis and canopy transpiration of rice crop simulated under the default scenario (SDs of the mean of 31 years in parentheses) for the present climate and the 2050 climate, under either potential or water-limited environments, in three representative sites*

Site	Los Baños (tropics)				Nanjing (subtropics)				Shizukuishi (temperate)			
Production level	Potential		Water limited		Potential		Water limited		Potential		Water limited	
Climate	Present	2050	Present	2050	Present	2050	Present	2050	Present	2050	Present	2050
Days to flowering	80.6 (1.8)	76.2 (1.2)	–	–	98.3 (2.2)	95.7 (1.0)	–	–	98.7 (5.8)	87.0 (4.4)	–	–
Days to maturity	110.7 (2.0)	105.2 (1.3)	–	–	143.6 (7.6)	133.0 (2.2)	–	–	133.4 (14.8)	113.8 (5.8)	–	–
Crop mass (g DM m^{-2})	1979.9 (55.4)	2141.7 (59.0)	1538.2 (60.4)	1644.8 (69.0)	2246.1 (93.1)	2420.3 (109.5)	1662.4 (108.4)	1782.9 (104.7)	1694.3 (65.5)	1803.4 (73.4)	1193.5 (104.6)	1272.6 (74.9)
Canopy photosynthesis (g CO_2 m^{-2})	5225.8 (145.7)	5598.9 (157.2)	4408.3 (130.5)	4600.7 (147.2)	5914.8 (231.7)	6330.9 (286.6)	4793.3 (185.9)	5011.2 (169.8)	4510.6 (153.1)	4702.0 (152.8)	3543.9 (218.3)	3668.0 (142.9)
Canopy transpiration (mm H_2O)	435.7 (25.4)	413.8 (18.9)	177.8 (3.6)	168.1 (3.1)	468.5 (37.3)	470.6 (33.4)	167.1 (4.3)	167.2 (3.2)	357.2 (20.0)	328.2 (19.8)	121.7 (10.3)	109.3 (5.6)
WUE[b] (g m^{-2} mm^{-1})	5.1	6.0	9.7	11.0	5.6	6.1	11.2	11.9	5.3	6.1	11.4	13.4

–, simulations assumed that drought had no impact on phenological development, so the predicted phenology was the same under water-limited as under the potential production level.
[a] Water use efficiency, defined as total crop mass production divided by the amount of water transpired during the growth season.

(Yin and Struik, 2008), we showed that a low g_{bs} alone would increase rice yield in the tropics by ~25%. However, that analysis used an arbitrarily low g_{bs} and a version of the C_4 model that assumes an H^+:ATP ratio of 3, whereas a recent analysis suggested that this ratio is most probably 4 (Yin and Struik, 2012), suggesting that the model version Yin and Struik (2008) used may have underestimated quantum requirement for the C_4 CCM. From our present analysis, even with the complete C_4 mechanism, its advantage over the C_3 default was simulated to be >50% only under the combination of water limitation and the present climate; for other conditions, its advantage ranged between 22% and 40% (Table 5).

As engineering for the complete Kranz anatomy is challenging, the CCM in cyanobacteria, which is probably less expensive energetically, has been suggested as an obvious alternative to engineer (Price *et al.*, 2011, 2013; Furbank *et al.*, 2015). Our simulation showed that the simplest form for the cyanobacterial CCM with bicarbonate transporters, Route 7, had a marginal advantage (Table 5). Pengelly *et al.*, (2014) showed that tobacco plants transformed with the BicA transporter had no discernible effect on CO_2 assimilation rates, suggesting that BicA was either not located or not activated correctly. Our simulation (Table 5) showed that a more elaborate cyanobacterial CCM, where the carboxysome shell proteins were expressed to enrich the CO_2 level around Rubisco in chloroplasts (Route 8), had a higher advantage than the equivalent C_4 CCM (Route 5), largely because of a lower ATP cost assumed for the cyanobacterial CCM. However, its benefit was lower than from the complete C_4 mechanism, namely Route 6, which includes the additional mechanism that C_4 plants have a considerably high carboxylation rate per unit leaf N (Evans and von Caemmerer, 2000; Makino *et al.*, 2003). The complete cyanobacterial mechanism (Route 9), which has the low energy cost for the CCM as well as the high carboxylation and e^- transport capacity per unit N (presumably as high as for C_4 plants), was the only route that could bring an advantage of ≥50% under any environmental conditions (Table 5). However, as the exact ATP cost for the cyanobacterial CCM is uncertain, the simulated benefits of Routes 7–9 should be considered as tentative and their real benefits might be lower (Supplementary Text 5).

Effects of enhanced leaf photosynthesis on some other crop traits

The benefit from all routes for simulated season-long canopy photosynthesis ($A_{canopy,s}$), shown in the upper rows of Fig. 3, differed from that shown in Table 5 for aboveground mass. This difference suggests that other traits were also affected by altered photosynthesis. Aboveground mass can be calculated as:

$$(PAR_{int} \times PLUE - RESP)\,(1 - F_{root}) - SENES$$

where PAR_{int} is the season-long intercepted PAR by the crop (MJ m^{-2}), PLUE is the overall photosynthetic light use efficiency (= $A_{canopy,s}/PAR_{int}$, g CO_2 MJ^{-1} PAR), RESP is season-long crop respiration (g CO_2 m^{-2}), F_{root} is fraction of mass for roots,

Table 5. *The percentage increase of the 31 year average aboveground mass by nine photosynthesis-enhancing routes, relative to that shown in Table 4 for the default route, in rice crop simulated for the present climate and the 2050 climate, under either potential or water stress environments, in three representative sites*

Site		Los Baños (tropics)				Nanjing (subtropics)				Shizukuishi (temperate)			
Production level		Potential		Water limited		Potential		Water limited		Potential		Water limited	
Climate		Present	2050	Present	2050	Present	2050	Present	2050	Present	2050	Present	2050
Route[a]	1	4.3	2.5	4.8	3.1	4.2	2.6	4.5	4.1	4.3	2.7	4.5	4.1
	2	8.8	8.0	7.5	6.8	9.3	8.5	11.7	9.7	9.2	8.1	11.0	9.2
	3	12.9	9.9	13.6	12.5	14.0	10.8	16.8	13.8	13.5	10.2	15.5	14.0
	4	10.4	4.1	12.4	6.4	8.0	3.9	11.8	6.2	14.8	8.3	19.2	10.4
	5	7.6	–0.8	26.6	13.6	5.0	–2.4	24.5	11.6	7.0	–0.7	26.6	14.9
	6	38.0	23.1	51.2	33.8	33.0	21.9	50.5	34.1	39.8	25.4	54.5	36.0
	7	5.4	1.6	9.1	5.2	4.5	0.8	10.6	6.0	5.5	2.1	11.3	7.7
	8	17.9	10.5	39.7	28.7	18.1	10.7	39.9	27.9	19.1	11.3	38.7	28.1
	9	70.1	57.5	78.5	61.2	63.2	51.3	74.8	57.9	60.8	49.0	73.8	57.4

[a] Route numbers correspond to those defined in Table 2.

and SENES is aboveground mass lost after leaf senescence (g DM m^{-2}). We obtained the data for these five traits from the GECROS output, and calculated the percentage change of each of these traits for each route relative to the C_3 default (Fig. 3).

The enhanced leaf photosynthesis from most routes also resulted in increased PAR_{int}, although to a small extent only, up to a maximum of 8.3% (Fig. 3). As a result, the percentage increase in PLUE by the routes was generally slightly lower than that in $A_{canopy,s}$ (Fig. 3). The increased PAR_{int} stemmed from an increased LAI in the early growth phase (results not shown), in line with the recent result of Kromdijk *et al.*, (2016) showing that increased leaf photosynthesis also resulted in increased leaf area. The increased canopy photosynthesis, on the one hand, increased the component of growth respiration; on the other hand, it decreased the component of maintenance respiration which is modelled in GECROS dependent on crop N status. The net result is that most routes decreased RESP (Fig. 3). The simulated F_{root} generally became higher with photosynthesis-enhancing routes (Fig. 3), as expected from the classical functional equilibrium theory (Brouwer, 1983). However, in the presence of water limitation, F_{root} could be lower compared with the default values, probably because the crop maintained a comparatively high N status under drought. Because a higher photosynthesis resulted in a lower N:C ratio in the crop and GECROS modelled leaf senescence depending on the relative magnitude of N- and C-determined LAI, the most effective enhancing routes, such as Routes 6 and 9, resulted in increased leaf senescence (Fig. 3). This simulation result is in analogy to the faster senescence and reduced LAI in later stages of development for C_3 crops grown under elevated [CO_2] in FACE experiments (e.g. Kim *et al.*, 2003). Sinclair *et al.*, (2004) simulated that a 33% increase in leaf photosynthesis may translate into only a 5% increase in soybean grain yield, or a –6% change in grain yield in the absence of additional N, presumably associated with more leaf senescence. Long *et al.*, (2006) reported experimentally a lower than expected crop yield stimulation with rising [CO_2].

Next, we evaluated the extent to which these secondary effects also contributed to differences in the simulated aboveground mass. This was done from the difference in the significance level of individual terms of multiple linear regression of aboveground mass versus PAR_{int}, PLUE, RESP, F_{root}, and SENES (Table 6). Although the decreasing effect of SENES on mass could not be identified (because of the collinearity between mass and SENES), the significant effect of the other four terms (PLUE, PAR_{int}, RESP, and F_{root}) was well estimated. While the primary PLUE had the strongest effect under both potential and water-limited conditions, the secondary PAR_{int} always had the second strongest effect. These results on the importance of the secondary effects on crop-level traits suggest that most existing simulation studies on assessing the impact of engineering photosynthetic targets are incomplete, because computation was only done for leaf photosynthesis (e.g. McGrath and Long, 2014) or for canopy photosynthesis (Zhu *et al.*, 2004; Song *et al.*, 2013).

Assessing the importance of individual biochemical targets

While secondary traits were affected, after all one would assess how the primary PLUE is affected by individual biochemical targets or parameters of photosynthesis. We regressed PLUE against individual photosynthetic parameters, with site included as covariate in the regression to remove any effect of possible site differences.

The regression analysis based on simulation results using the C_3 model (Routes 1–3 plus the default) indicated that manipulating $S_{c/o}$ affected PLUE more than manipulating g_m (results not shown), consistent with the result that the percentage change in PLUE by Route 2 was higher than that by Route 1 (Fig. 3). However, the relative impact of manipulating $S_{c/o}$ and g_m depends on the extent to which they could actually be changed. Furthermore, an improvement in $S_{c/o}$ may be at the cost of decreasing V_{cmax}, because of the often observed negative correlation between Rubisco

Trait	Route	Los Baños				Nanjing				Shizukuishi			
		Potential		Water-limted		Potential		Water-limited		Potential		Water-limited	
		Present	2050	Present	2050	Present	2050	Present	2050	Present	2050	Present	2050
$A_{canopy,s}$	1	5.1	3.0	3.1	1.8	4.8	3.2	2.3	2.5	3.4	2.5	3.0	3.0
	2	8.4	7.6	4.4	3.7	9.0	8.5	6.7	5.7	6.9	7.2	7.1	6.1
	3	14.1	10.5	8.2	7.4	15.0	11.9	10.3	8.8	11.3	10.0	10.1	9.4
	4	5.1	-0.8	5.2	1.9	3.2	-1.1	5.4	2.2	7.9	3.1	10.3	4.8
	5	8.1	-0.7	16.1	7.9	5.4	-2.4	14.6	6.5	5.3	-0.3	16.9	9.7
	6	29.0	15.4	31.3	19.8	27.9	16.2	31.7	20.3	31.4	19.0	31.6	20.4
	7	5.6	1.0	5.6	3.0	3.8	0.2	6.1	3.7	4.1	1.5	7.6	5.3
	8	20.9	11.6	26.6	18.6	21.5	12.5	26.8	18.5	18.4	11.5	24.5	18.3
	9	59.8	43.5	52.1	38.6	56.8	41.4	50.3	37.4	57.6	44.7	47.0	35.6
PAR_{int}	1	0.0	-0.1	-0.4	-0.5	0.0	0.0	-0.2	0.1	-0.3	-0.2	0.6	0.5
	2	0.7	0.5	-0.3	-0.6	0.7	0.5	0.4	0.2	0.2	0.5	2.5	1.2
	3	0.7	0.4	-0.8	-0.5	0.7	0.4	0.4	0.3	0.2	0.3	2.9	1.6
	4	3.3	2.3	1.3	1.4	2.2	1.7	1.7	1.6	4.2	4.1	5.8	3.4
	5	0.7	0.3	-0.8	-0.1	0.6	0.1	1.4	0.8	0.4	0.6	5.0	2.1
	6	4.6	2.7	2.3	2.0	3.6	2.5	3.9	3.0	5.4	4.8	9.1	5.6
	7	0.4	0.3	-0.8	-0.2	-0.8	0.0	0.2	0.4	0.0	0.1	1.8	0.7
	8	0.8	0.3	-0.7	0.1	1.0	0.4	1.8	1.2	0.7	0.3	6.1	2.3
	9	5.7	4.4	3.0	3.1	3.6	3.5	4.0	3.7	4.5	4.1	8.3	4.9
PLUE	1	5.1	3.1	3.5	2.3	4.7	3.2	2.5	2.4	3.7	2.8	2.4	2.5
	2	7.7	7.0	4.7	4.3	8.2	7.9	6.2	5.5	6.6	6.7	4.5	4.8
	3	13.3	10.1	9.0	7.9	14.1	11.4	9.9	8.4	11.1	9.7	7.1	7.7
	4	1.7	-3.0	3.9	0.5	0.9	-2.7	3.7	0.6	3.6	-1.0	4.3	1.4
	5	7.4	-1.0	16.9	8.0	4.7	-2.4	13.0	5.6	4.9	-0.8	11.3	7.5
	6	23.4	12.3	28.4	17.5	23.5	13.4	26.7	16.8	24.7	13.6	20.6	14.1
	7	5.1	0.7	6.4	3.2	4.7	0.2	5.9	3.3	4.0	1.4	5.7	4.5
	8	19.9	11.3	27.5	18.5	20.2	12.0	24.5	17.0	17.6	11.2	17.4	15.7
	9	51.2	37.4	47.7	34.5	51.4	36.6	44.5	32.5	50.9	38.9	35.8	29.3
RESP	1	0.0	0.1	-0.1	-0.9	0.0	0.2	-1.5	-0.7	1.0	0.5	0.7	1.5
	2	-1.3	-0.7	-1.2	-2.9	-0.5	0.0	-2.2	-4.2	0.5	0.1	2.3	2.1
	3	-0.3	0.1	-1.4	-2.6	0.1	0.8	-4.1	-5.6	1.2	0.3	2.7	3.6
	4	-7.7	-6.4	-6.6	-5.8	-7.2	-6.7	-5.3	-5.4	-6.5	-6.5	-0.8	-2.1
	5	-1.8	-0.8	-5.7	-4.0	-2.0	-1.4	-9.6	-6.5	0.4	0.3	3.9	2.2
	6	-7.8	-7.0	-14.3	-12.8	-5.3	-4.9	-18.0	-16.9	-7.7	-8.1	0.2	-1.2
	7	-1.1	-1.3	-1.2	-1.6	-2.5	-1.1	-2.1	-1.5	0.4	-0.5	2.3	2.0
	8	0.3	0.0	-8.4	-8.5	0.9	0.6	-12.9	-12.6	0.8	0.0	5.3	4.1
	9	-2.1	-3.6	-14.4	-16.4	1.4	-0.4	-19.1	-19.9	-0.9	-2.3	1.2	0.4
F_{root}	1	29.9	12.9	-5.1	-2.7	17.7	10.8	-4.7	-0.7	-0.6	6.5	-2.1	-2.0
	2	34.9	48.7	-5.4	-14.0	62.7	77.3	-9.8	-6.5	-1.1	12.7	-7.2	19.8
	3	63.8	64.8	-10.7	-17.4	90.7	94.3	3.5	5.1	15.4	29.1	-9.3	15.4
	4	-3.4	-6.7	-18.8	-21.8	21.8	17.6	-14.3	-17.3	-13.6	-22.2	-22.3	6.3
	5	44.5	25.7	-6.5	-16.3	65.4	48.5	16.1	-1.8	-0.6	-1.4	-17.7	13.6
	6	46.2	27.0	17.3	1.9	88.6	63.5	48.7	25.8	57.8	31.4	-37.5	-17.4
	7	28.5	26.7	-5.4	-11.5	33.0	49.7	-6.5	-10.0	-2.7	-4.7	-5.3	23.6
	8	71.2	72.6	26.8	11.6	124.1	102.2	51.0	34.9	55.3	38.9	-24.8	1.7
	9	91.9	48.5	43.5	17.8	121.4	82.5	70.2	44.7	129.7	95.1	-14.6	-8.9
SENES	1	2.3	1.3	14.4	10.7	0.9	0.2	9.2	3.4	7.1	2.7	4.3	-9.2
	2	7.2	7.4	26.1	23.5	9.7	5.5	12.3	13.4	17.7	8.1	-1.8	-5.1
	3	10.6	8.6	37.3	26.1	8.4	5.3	18.0	15.5	19.9	8.8	6.5	-10.6
	4	19.1	9.7	56.1	25.4	14.6	9.6	21.1	11.9	41.0	20.2	28.9	16.1
	5	7.4	-1.8	78.4	32.3	1.5	-2.9	38.0	16.4	12.9	-7.0	11.4	5.6
	6	37.5	25.8	119.3	59.6	24.6	18.8	59.4	40.1	66.7	38.7	70.1	50.9
	7	4.9	0.6	32.8	14.7	12.9	3.1	10.5	3.7	10.0	3.5	3.4	-6.4
	8	15.2	9.2	100.5	50.7	8.0	5.7	55.9	35.8	22.3	11.2	27.2	20.9
	9	52.8	44.9	143.2	89.9	35.3	28.9	86.1	61.6	74.4	55.3	77.2	71.3
WUE	1	2.0	1.2	4.6	3.6	1.4	1.1	4.4	3.4	0.6	0.9	4.0	3.3
	2	7.6	6.1	7.9	7.5	7.3	6.2	11.2	9.8	5.9	5.5	9.1	7.3
	3	9.3	6.9	13.9	12.1	8.7	7.1	16.8	14.2	6.9	6.5	13.1	11.0
	4	31.6	25.4	13.7	7.7	28.3	22.5	11.0	6.8	31.1	24.1	15.7	8.4
	5	36.7	28.3	32.7	18.0	33.3	23.9	29.4	15.4	31.2	24.5	26.1	15.2
	6	48.3	40.3	53.8	36.0	43.7	36.0	51.0	36.4	47.0	38.4	43.3	29.0
	7	31.9	27.9	12.9	8.8	27.8	24.3	13.2	8.5	29.1	26.0	13.1	8.9
	8	42.0	39.4	49.0	35.2	42.1	35.9	46.9	34.3	41.2	36.2	35.8	26.3
	9	61.3	54.5	82.2	62.1	55.5	48.7	75.7	60.2	60.2	54.2	63.3	48.5

Fig. 3. Heat map for the percentage change (%) of the 31 year average trait value for each of the nine photosynthesis-enhancing routes (route numbers defined in Table 2), relative to that for the default route, in a rice crop simulated for the present climate and the 2050 climate, under either potential or water-limited environments, at three representative sites. Traits shown are: $A_{canopy,s}$, season-long canopy photosynthesis; PAR_{int}, season-long intercepted PAR; PLUE, overall photosynthetic light use efficiency defined as $A_{canopy,s}$ divided by PAR_{int}; RESP, season-long crop respiration; F_{root}, fraction of mass for roots; SENES, shoot mass lost due to leaf senescence; and WUE, water use efficiency. (Colours: white for no change, green for decrease, red for increase, and colour intensity for the magnitude of decrease or increase.)

$S_{c/o}$ and carboxylase turnover rate (e.g. Kubien *et al.*, 2008; Perdomo *et al.*, 2015). This negative correlation was not considered here, in view of the fact that the non-green alga *G. monilis* has a high $S_{c/o25}$ while maintaining a Rubisco turnover rate similar to C_3 plants (Whitney *et al.*, 2001). The impact of the trade-off between Rubisco $S_{c/o}$ and carboxylase turnover on canopy photosynthesis was analysed by Zhu *et al.*, (2004).

Our simulations using the C_4 model (Routes 4–9) involved changes in values of a set of parameters. The most important ones are χ_{gbs25} (which determines the effectiveness of the CCM), φ (extra ATP requirement for the CCM, which determines the required f_{cyc} and, therefore, light-limited photosynthetic efficiency), and $\chi_{Vcmax25}$ or χ_{Jmax25} (which determine light-saturated photosynthetic capacity). Other parameters (e.g. some C_3 parameters used for Route 5) had little impact on the shape and values of light response curves (results not shown). We therefore conducted the analysis of regressing PLUE versus χ_{gbs25}, 3 + φ (total ATP requirement per mol CO_2 assimilated, ATP_{req}), and χ_{Jmax25} (Table 7). There was little effect of sites on PLUE. All three parameters were important for any production level–climate combination. Comparatively, the CCM parameter χ_{gbs25} became most important for water-limited production, because a more effective CCM to elevate the CO_2 level around Rubisco can more effectively overcome the negative effect of low C_i under drought. Under the potential production, especially combined with high [CO_2] of the 2050 climate, the photosynthetic capacity parameter χ_{Jmax25} and quantum efficiency parameter ATP_{req} were comparatively more important (Table 7). These results suggest that photosynthetic capacity, quantum efficiency, and CCM strength all need improving in order to turbocharge canopy photosynthesis. Based on natural variation of leaf photosynthesis, Gu *et al.*, (2014*a*) showed that quantum efficiency parameters had even higher effects than capacity parameters on rice productivity.

Table 6. *The coefficients (with probability of significance in parentheses) of linear regression of 31 year average simulated aboveground mass against the simulated values of five component traits, for either potential or water-limited environments, or using the pooled data for the two environments*

The five component traits are: PAR_{int}, season-long intercepted PAR; PLUE, overall photosynthetic light use efficiency defined as season-long canopy photosynthesis divided by PAR_{int}; RESP, season-long crop respiration; F_{root}, fraction of mass for roots; SENES, aboveground mass lost due to leaf senescence. Linear regression is given as: $Y = b_0 + b_1 \cdot PAR_{int} + b_2 \cdot PLUE + b_3 \cdot RESP + b_4 \cdot F_{root} + b_5 \cdot SENES$

Coefficient (unit)	Potential	Water-limited	Pooled data
b_0 (g DM m^{-2})	–3435.24 (5.92×10^{-18})	–1907.22 (5.34×10^{-32})	–1751.43 (1.57×10^{-34})
b_1 (g DM MJ^{-1} PAR)	4.495 (2.00×10^{-24})	3.064 (7.19×10^{-40})	3.342 (9.92×10^{-42})
b_2 [g DM m^{-2} (g CO_2 MJ^{-1} PAR)$^{-1}$]	415.65 (9.36×10^{-35})	339.49 (3.47×10^{-48})	328.83 (1.32×10^{-70})
b_3 [g DM (g CO_2)$^{-1}$]	–0.2635 (0.045)	–0.5735 (6.53×10^{-22})	-0.7445 (1.22×10^{-23})
b_4 (g DM m^{-2})	–3967.04 (5.05×10^{-13})	–539.44 (0.001)	-1245.07 (2.92×10^{-8})
b_5 (g DM g^{-1} DM)	–1.1938 (0.153)	1.6387 (6.84×10^{-6})	1.9219 (0.001)
R^2	0.992	0.999	0.993
Data points	60	60	120

Table 7. *The coefficients with their probability of significance of linear regression of 31 year average simulated PLUE (overall photosynthetic light-use efficiency as defined in Table 6) against three biochemical parameters (χ_{gbs25}, ATP_{req}, and χ_{Jmax25}, representing the strength of the CCM, quantum requirement, and photosynthetic capacity, respectively) used in the C_4 photosynthesis model, for four cases where potential or water-limited environments were combined with present or 2050 climate conditions*

	Potential level				Water-limited level			
	Present climate		2050 climate		Present climate		2050 climate	
	Coefficient	Probability	Coefficient	Probability	Coefficient	Probability	Coefficient	Probability
Intercept	11.674	1.45×10^{-11}	12.108	2.67×10^{-12}	9.019	2.31×10^{-12}	9.385	1.49×10^{-14}
Nanjing[a]	0.097	0.56	0.102	0.50	–0.078	0.48	–0.112	0.15
Shizukuishi[a]	0.167	0.32	0.415	0.01	–0.200	0.09	–0.051	0.49
χ_{gbs25}	–12.751	1.64×10^{-7}	–10.574	3.91×10^{-7}	–10.262	1.84×10^{-8}	–8.406	2.23×10^{-9}
ATP_{req}[b]	–1.237	1.22×10^{-7}	–1.244	3.46×10^{-8}	–0.659	1.24×10^{-6}	–0.676	1.40×10^{-8}
χ_{Jmax25}	0.0162	7.37×10^{-8}	0.0150	5.12×10^{-8}	0.0083	1.22×10^{-6}	0.0072	7.76×10^{-8}
R^2	0.963		0.965		0.961		0.976	
Data points	18		18		18		18	

[a] Site was included as the covariate in regression, with Los Baños as the reference having a coefficient of zero.
[b] Total ATP requirement per CO_2 assimilated (= 3 + φ), i.e. 5 for C_4 photosynthesis and 3.75 for cyanobacterial photosynthesis (see the text).

Concluding remarks

We simulated the likely impact of major routes in ongoing programmes using transgenic technology to improve photosynthesis (Table 2). Our analysis showed that improving leaf photosynthesis can result in an increased rice mass production to a different extent (Table 5), thereby also resulting in different improvements in resource use efficiency such as WUE (Fig. 3). However, to supercharge photosynthesis significantly, engineering for a single improvement route can hardly be effective. Some single routes may be counter-productive at the canopy level. For example, installing C_4 biochemistry, if not combined with an effective CCM, is only beneficial for upper leaves of the canopy, while it has no or even a negative impact for lower shaded leaves because such a mechanism requires extra ATP for the C_4 cycle. Note that the standard C_4 model of von Caemmerer and Furbank (1999) for e^- transport limitation does not explicitly consider the increased cyclic e^- transport due to the extra ATP costs relative to C_3 photosynthesis, and, therefore, cannot recognize the little advantage of C_4 photosynthesis under shade. Similarly, the simulation by McGrath and Long (2014) in assessing the potential of cyanobacterial CCM took no account of the extra ATP required by bicarbonate transporters. Our simulation also showed that manipulating photosynthesis may result in unwanted secondary effects on some traits at crop level (e.g. inducing faster senescence if nutrient uptake is not increased). Therefore, the beneficial effect of the single route for high photosynthesis on increasing crop productivity may have previously been overestimated. To supercharge crop productivity, combined routes for improved CCM, photosynthetic capacity, and quantum efficiency are required.

Supplementary Data

Supplementary data are available at *JXB* online.

Fig. S1. Simulated versus observed relationships between A and g_s.

Text 1. Analytical solution to the cubic equation as a result of combined stomatal conductance, CO_2 diffusion, and biochemical leaf photosynthesis models.

Text 2. Revising the C_4 photosynthesis model for simulating the cyanobacterial CCM.

Text 3. Analytical solution to the quadratic equation as a result of combined CO_2

Text 4. Analysis with respect to temperature response parameters of C_4 enzyme kinetics.

Text 5. Sensitivity analysis with respect to ATP cost for the cyanobacterial CCM.

Text 6. Description of the crop model GECROS (version 4.0).

Acknowledgements

This research is financed in part by the BioSolar Cells open innovation consortium, supported by the Dutch Ministry of Economic Affairs, Agriculture and Innovation. We thank the AgMIP-Rice team for the weather data used in this study.

References

Bernacchi CJ, Pimentel C, Long SP. 2003. *In vivo* temperature response functions of parameters required to model RuBP-limited photosynthesis. Plant, Cell and Environment **26,** 1419–1430.

Bernacchi CJ, Portis AR, Nakano H, von Caemmerer S, Long SP. 2002. Temperature response of mesophyll conductance. Implications for the determination of Rubisco enzyme kinetics and for limitations to photosynthesis in vivo. Plant Physiology **130,** 1992–1998.

Bernacchi CJ, Singsaas EL, Pimentel C, Portis AR Jr, Long SP. 2001. Improved temperature response functions for models of Rubisco-limited photosynthesis. Plant, Cell and Environment **24,** 253–259.

Boote KJ, Jones JW, White JW, Asseng S, Lizaso JI. 2013. Putting mechanisms into crop production models. Plant, Cell and Environment **36,** 1658–1672.

Boyd RA, Gandin A, Cousins AB. 2015. Temperature responses of C_4 photosynthesis: biochemical analysis of rubisco, phosphoenolpyruvate carboxylase, and carbonic anhydrase in *Setaria viridis*. Plant Physiology **169,** 1850–1861.

Brouwer R. 1983. Functional equilibrium: sense or nonsense? Netherlands Journal of Agricultural Science **31,** 335–348.

Cai C, Yin X, He S, *et al*. 2016. Responses of wheat and rice to factorial combinations of ambient and elevated CO_2 and temperature in FACE experiments. Global Change Biology **22,** 856–874.

Chen CP, Sakai H, Tokida T, Usui Y, Nakamura H, Hasegawa T. 2014. Do the rich always become richer? Characterizing the leaf physiological response of the high-yielding rice cultivar Takanari to free-air CO_2 enrichment. Plant and Cell Physiology **55,** 381–391.

Cousins AB, Ghannoum O, von Caemmerer S, Badger MR. 2010. Simultaneous determination of Rubisco carboxylase and oxygenase kinetic parameters in Triticum aestivum and Zea mays using membrane inlet mass spectrometry. Plant, Cell and Environment **33,** 444–452.

de Pury DGG, Farquhar GD. 1997. Simple scaling of photosynthesis from leaves to canopies without the errors of big-leaf models. Plant, Cell and Environment **20,** 537–557.

Driever SM, Lawson T, Andralojc PJ, Raines CA, Parry MA. 2014. Natural variation in photosynthetic capacity, growth, and yield in 64 field-grown wheat genotypes. Journal of Experimental Botany **65,** 4959–4973.

Evans JR, von Caemmerer S. 2000. Would C4 rice produce more biomass than C_3 rice? In: **Sheehy JE, Mitchell PL, Hardy B**, eds. Redesigning rice photosynthesis to increase yield. Los Baños, the Philippines: International Rice Research Institute, 53–71.

Farquhar GD, von Caemmerer S, Berry JA. 1980. A biochemical model of photosynthetic CO_2 assimilation in leaves of C_3 species. Planta **149,** 78–90.

Fischer RA, Byerlee D, Edmeades GO. 2014. Crop yields and global food security: will yield increase continue to feed the world? ACIAR Monograph No. 158. Canberra: Australian Centre for International Agricultural Research.

Flexas J, Niinemets U, Gallé A, *et al*. 2013. Diffusional conductances to CO_2 as a target for increasing photosynthesis and photosynthetic water-use efficiency. Photosynthesis Research **117,** 45–59.

Flood PJ, Harbinson J, Aarts MG. 2011. Natural genetic variation in plant photosynthesis. Trends in Plant Science **16,** 327–335.

Fridlyand L, Kaplan A, Reinhold L. 1996. Quantitative evaluation of the role of a putative CO_2-scavenging entity in the cyanobacterial CO_2-concentrating mechanism. Bio Systems **37,** 229–238.

Furbank RT, Jenkins CLD, Hatch MD. 1990. C_4 photosynthesis: quantum requirement, C_4 acid overcycling and Q-cycle involvement. Australian Journal of Plant Physiology **17,** 1–7.

Furbank RT, Quick WP, Sirault XRR. 2015. Improving photosynthesis and yield potential in cereal crops by targeted genetic manipulation: prospects, progress and challenges. Field Crops Research **182,** 19–29.

Genty B, Harbinson J. 1996. Regulation of light utilization for photosynthetic electron transport. In: **Baker NR**, ed. Photosynthesis and the environment. Dordrecht, The Netherlands: Kluwer Academic Publishers, 67–99.

Goudriaan J. 1986. A simple and fast numerical method for the computation of daily totals of crop photosynthesis. Agricultural and Forest Meteorology **38,** 249–254.

Goudriaan J, van Laar HH. 1994. Modelling potential crop growth processes. Dordrecht, The Netherlands: Kluwer Academic Publishers.

Gu J, Yin X, Stomph TJ, Struik PC. 2014*a*. Can exploiting natural genetic variation in leaf photosynthesis contribute to increasing rice productivity? A simulation analysis. Plant, Cell and Environment **37,** 22–34.

Gu J, Yin X, Stomph TJ, Wang H, Struik PC. 2012. Physiological basis of genetic variation in leaf photosynthesis among rice (*Oryza sativa* L.) introgression lines under drought and well-watered conditions. Journal of Experimental Botany **63,** 5137–5153.

Gu J, Yin X, Zhang C, Wang H, Struik PC. 2014*b*. Linking ecophysiological modelling with quantitative genetics to support marker-assisted crop design for improved yields of rice (*Oryza sativa*) under drought stress. Annals of Botany **114,** 499–511.

Hanson MR, Lin MT, Carmo-Silva AE, Parry MA. 2016. Towards engineering carboxysomes into C_3 plants. The Plant Journal **87,** 38–50.

Harley PC, Thomas RB, Reynolds JF, Strain BR. 1992. Modelling photosynthesis of cotton grown in elevated CO_2. Plant, Cell and Environment **15,** 271–282.

June T, Evans JR, Farquhar GD. 2004. A simple new equation for the reversible temperature dependence of photosynthetic electron transport: a study on soybean leaf. Functional Plant Biology **31,** 275–283.

Kebeish R, Niessen M, Thiruveedhi K, Bari R, Hirsch HJ, Rosenkranz R, Stäbler N, Schönfeld B, Kreuzaler F, Peterhänsel C. 2007. Chloroplastic photorespiratory bypass increases photosynthesis and biomass production in Arabidopsis thaliana. Nature Biotechnology **25,** 593–599.

Kim HY, Lieffering M, Kobayashi K, Okada M, Miura S. 2003. Seasonal changes in the effects of elevated CO_2 on rice at three levels of nitrogen supply: a free air CO_2 enrichment (FACE) experiment. Global Change Biology **9,** 826–837.

Koester RP, Nohl BM, Diers BW, Ainsworth EA. 2016. Has photosynthetic capacity increased with 80 years of soybean breeding? An examination of historical soybean cultivars. Plant, Cell and Environment **39,** 1058–1067.

Kromdijk J, Long SP. 2016. One crop breeding cycle from starvation? How engineering crop photosynthesis for rising CO_2 and temperature could be one important route to alleviation. Proceedings of the Royal Society B: Biological Sciences **283,** 20152578.

Kromdijk J, Głowacka K, Leonelli L, Gabilly ST, Iwai M, Niyogi KK, Long SP. 2016. Improving photosynthesis and crop productivity by accelerating recovery from photoprotection. Science **354,** 857–861.

Kubien DS, Whitney SM, Moore PV, Jesson LK. 2008. The biochemistry of Rubisco in Flaveria. Journal of Experimental Botany **59,** 1767–1777.

Leuning R. 1995. A critical appraisal of a combined stomatal–photosynthesis model for C_3 plants. Plant, Cell and Environment **18,** 339–355.

Li T, Hasegawa T, Yin X, *et al*. 2015. Uncertainties in predicting rice yield by current crop models under a wide range of climatic conditions. Global Change Biology **21,** 1328–1341.

Lin MT, Occhialini A, Andralojc PJ, Devonshire J, Hines KM, Parry MA, Hanson MR. 2014. β-Carboxysomal proteins assemble into highly organized structures in Nicotiana chloroplasts. The Plant Journal **79,** 1–12.

Long BM, Rae BD, Rolland V, Förster B, Price GD. 2016. Cyanobacterial CO_2-concentrating mechanism components: function and prospects for plant metabolic engineering. Current Opinion in Plant Biology **31,** 1–8.

Long SP, Ainsworth EA, Leakey AD, Nösberger J, Ort DR. 2006. Food for thought: lower-than-expected crop yield stimulation with rising CO_2 concentrations. Science **312,** 1918–1921.

Long SP, Marshall-Colon A, Zhu XG. 2015. Meeting the global food demand of the future by engineering crop photosynthesis and yield potential. Cell **161,** 56–66.

Long SP, Zhu XG, Naidu SL, Ort DR. 2006. Can improvement in photosynthesis increase crop yields? Plant, Cell and Environment **29,** 315–330.

Makino A, Sakuma H, Sudo E, Mae T. 2003. Differences between maize and rice in N-use efficiency for photosynthesis and protein allocation. Plant and Cell Physiology **44,** 952–956.

McGrath JM, Long SP. 2014. Can the cyanobacterial carbon-concentrating mechanism increase photosynthesis in crop species? A theoretical analysis. Plant Physiology **164,** 2247–2261.

Monteith JL. 1973. Principles of environmental physics. London: Edward Arnold.

Miflin B. 2000. Crop improvement in the 21st century. Journal of Experimental Botany **51,** 1–8.

Morison JI, Gifford RM. 1983. Stomatal sensitivity to carbon dioxide and humidity: a comparison of two C_3 and two C_4 grass species. Plant Physiology **71,** 789–796.

Murchie EH, Pinto M, Horton P. 2009. Agriculture and the new challenges for photosynthesis research. New Phytologist **181,** 532–552.

Nakamura N, Iwano M, Havaux M, Yokota A, Munekage YN. 2013. Promotion of cyclic electron transport around photosystem I during the evolution of NADP-malic enzyme-type C_4 photosynthesis in the genus Flaveria. New Phytologist **199,** 832–842.

Ort DR, Merchant SS, Alric J. *et al*. 2015. Redesigning photosynthesis to sustainably meet global food and bioenergy demand. Proceedings of the National Academy of Sciences, USA **112,** 8529–8536.

Parry MA, Reynolds M, Salvucci ME, Raines C, Andralojc PJ, Zhu XG, Price GD, Condon AG, Furbank RT. 2011. Raising yield potential of wheat. II. Increasing photosynthetic capacity and efficiency. Journal of Experimental Botany **62,** 453–467.

Pengelly JJ, Förster B, von Caemmerer S, Badger MR, Price GD, Whitney SM. 2014. Transplastomic integration of a cyanobacterial bicarbonate transporter into tobacco chloroplasts. Journal of Experimental Botany **65,** 3071–3080.

Perdomo JA, Cavanagh AP, Kubien DS, Galmés J. 2015. Temperature dependence of in vitro Rubisco kinetics in species of Flaveria with different photosynthetic mechanisms. Photosynthesis Research **124,** 67–75.

Price GD, Badger MR, von Caemmerer S. 2011. The prospect of using cyanobacterial bicarbonate transporters to improve leaf photosynthesis in C_3 crop plants. Plant Physiology **155,** 20–26.

Price GD, Pengelly JJ, Forster B, Du J, Whitney SM, von Caemmerer S, Badger MR, Howitt SM, Evans JR. 2013. The cyanobacterial CCM as a source of genes for improving photosynthetic CO_2 fixation in crop species. Journal of Experimental Botany **64,** 753–768.

Sadras VO, Lawson C. 2011. Genetic gain in yield and associated changes in phenotype, trait plasticity and competitive ability of South Australian wheat varieties released between 1958 and 2007. Crop and Pasture Science **62,** 533–549.

Sage RF. 2002. Variation in the k_{cat} of Rubisco in C_3 and C_4 plants and some implications for photosynthetic performance at high and low temperature. Journal of Experimental Botany **53,** 609–620.

Seemann JR, Badger MR, Berry JA. 1984. Variations in the specific activity of ribulose-1,5-bisphosphate carboxylase between species utilizing differing photosynthetic pathways. Plant Physiology **74,** 791–794.

Setter TL, Peng S, Kirk GJD, Virmani SS, Kropff MJ, Cassman KG. 1994. Physiological considerations and hybrid rice. In: **Cassman KG**, ed. Breaking the yield barrier. Proceedings of a workshop on rice yield potential in favorable environments. Los Baños, Philippines: IRRI, 39–62.

Shikanai T. 2007. Cyclic electron transport around photosystem I: genetic approaches. Annual Review of Plant Biology **58,** 199–217.

Sinclair TR, Horie T. 1989. Leaf nitrogen, photosynthesis, and crop radiation use efficiency: a review. Crop Science **29,** 90–98.

Sinclair TR, Purcell LC, Sneller CH. 2004. Crop transformation and the challenge to increase yield potential. Trends in Plant Science **9,** 70–75.

Singh J, Pandey P, James D, Chandrasekhar K, Achary VM, Kaul T, Tripathy BC, Reddy MK. 2014. Enhancing C_3 photosynthesis: an outlook on feasible interventions for crop improvement. Plant Biotechnology Journal **12,** 1217–1230.

Song Q, Zhang G, Zhu X-G. 2013. Optimal crop canopy architecture to maximise canopy photosynthetic CO_2 uptake under elevated CO_2—a theoretical study using a mechanistic model of canopy photosynthesis. Functional Plant Biology **40,** 109–124.

Tholen D, Boom C, Zhu XG. 2012. Opinion: prospects for improving photosynthesis by altering leaf anatomy. Plant Science **197,** 92–101.

von Caemmerer S. 2013. Steady-state models of photosynthesis. Plant, Cell and Environment **36,** 1617–1630.

von Caemmerer S, Furbank RT. 1999. Modeling C_4 photosynthesis. In: **Sage RF, Monson RK**, eds. C_4 plant biology. Toronto: Academic Press, 173–211.

von Caemmerer S, Furbank RT. 2003. The C_4 pathway: an efficient CO_2 pump. Photosynthesis Research **77,** 191–207.

von Caemmerer S, Quick WP, Furbank RT. 2012. The development of C_4 rice: current progress and future challenges. Science **336,** 1671–1672.

Walker BJ, VanLoocke A, Bernacchi CJ, Ort DR. 2016. The costs of photorespiration to food production now and in the future. Annual Review of Plant Biology **67,** 107–129.

Whitney SM, Baldet P, Hudson GS, Andrews TJ. 2001. Form I Rubiscos from non-green algae are expressed abundantly but not assembled in tobacco chloroplasts. The Plant Journal **26,** 535–547.

Wong SC, Cowan IR, Farquhar GD. 1985. Leaf conductance in relation to rate of CO_2 assimilation: I. Influence of nitrogen nutrition, phosphorus nutrition, photon flux density, and ambient partial pressure of CO_2 during ontogeny. Plant Physiology **78,** 821–825.

Yin X, Belay DW, van der Putten PE, Struik PC. 2014. Accounting for the decrease of photosystem photochemical efficiency with increasing irradiance to estimate quantum yield of leaf photosynthesis. Photosynthesis Research **122,** 323–335.

Yin X, Goudriaan J, Lantinga EA, Vos J, Spiertz JHJ. 2003. A flexible sigmoid function of determinate growth. Annals of Botany **91,** 361–371 (erratum in Annals of Botany 2003. 91, 753).

Yin X, Harbinson J, Struik PC. 2006. Mathematical review of literature to assess alternative electron transports and interphotosystem excitation partitioning of steady-state C_3 photosynthesis under limiting light. Plant, Cell and Environment **29,** 1771–1782.

Yin X, Struik PC. 2008. Applying modelling experiences from the past to shape crop systems biology: the need to converge crop physiology and functional genomics. New Phytologist **179,** 629–642.

Yin X, Struik PC. 2009. C_3 and C_4 photosynthesis models: an overview from the perspective of crop modelling. NJAS-Wageningen Journal of Life Sciences **57,** 27–38.

Yin X, Struik PC. 2012. Mathematical review of the energy transduction stoichiometries of C_4 leaf photosynthesis under limiting light. Plant, Cell and Environment **35,** 1299–1312.

Yin X, Struik PC, Romero P, Harbinson J, Evers JB, van der Putten PE, Vos J. 2009. Using combined measurements of gas exchange and chlorophyll fluorescence to estimate parameters of a biochemical C_3 photosynthesis model: a critical appraisal and a new integrated approach applied to leaves in a wheat (*Triticum aestivum*) canopy. Plant, Cell and Environment **32,** 448–464.

Yin X, Sun Z, Struik PC, Van der Putten PE, Van Ieperen W, Harbinson J. 2011. Using a biochemical C_4 photosynthesis model and combined gas exchange and chlorophyll fluorescence measurements to estimate bundle-sheath conductance of maize leaves differing in age and nitrogen content. Plant, Cell and Environment **34,** 2183–2199.

Yin X, van der Putten PE, Driever SM, Struik PC. 2016. Temperature response of bundle-sheath conductance in maize leaves. Journal of Experimental Botany **67,** 2699–2714.

Yin X, van Laar HH. 2005. Crop systems dynamics: an ecophysiological simulation model for genotype-by-environment interactions. Wageningen, The Netherlands: Wageningen Academic Publishers.

Yin X, van Oijen M, Schapendonk AHCM. 2004. Extension of a biochemical model for the generalized stoichiometry of electron transport limited C_3 photosynthesis. Plant, Cell and Environment **27,** 1211–1222.

Zhu X-G, Portis AR Jr, Long SP. 2004. Would transformation of C_3 crop plants with foreign Rubisco increase productivity? A computational analysis extrapolating from kinetic properties to canopy photosynthesis. Plant, Cell and Environment **27,** 55–165.